Journal of Sound and Vibration (2000) **229**(2), 355–375
Article No. jsvi.1999.2482, available online at http://www.idealibrary.com on IDEAL®

INCREASING THE NATURAL FREQUENCIES OF CIRCULAR DISKS USING INTERNAL CHANNELS

A. A. RENSHAW

Department of Mechanical Engineering, Columbia University, Mail Code 4703, *New York, NY 10027, U.S.A.*

(*Received* 8 *February* 1999, *and in final form* 28 *June* 1999)

This paper investigates a new design for computer disk drive disks that raises their natural frequencies. In this new design, a pattern of small, dense, internal channels or voids is distributed axisymmetrically about the midplane of the disk. These channels increase the natural frequencies of the disk by removing mass from the midplane of the disk while maintaining the coupling between the deflections of the upper and lower surfaces of the disk. This practice is commonly employed in I-beams and honeycombed sandwich panels, but the channeled geometry proposed here has not been previously considered or studied. This paper presents a detailed analytical model for a channeled disk, specifications for optimal channeled disk design, and experimental corroboration. Numerical results show that the natural frequencies of a properly channeled disk can be 10–100% higher than those of a uniform disk, depending on the size of the channels. The orientation of the channels does not significantly affect the natural frequencies, but, in the optimal design, the channels do not extend through the whole disk. Instead, they begin at an optimal, central, transition radius and radiate outward to the outer edge of the disk. Disks with this optimal channel design may be competitive with uniform thickness disks for disk drive applications in terms of both natural frequency and cost.

1. INTRODUCTION

Vibration reduction of high-speed rotating disks is a primary concern in the design of industrial circular saws and hard disk drives. In each technology, the design objective is the same: maximize the lowest natural frequency measured by a stationary observer. However, because of different performance requirements, there are many more techniques available for raising natural frequencies of circular saws than there are for disk drive disks. Saw natural frequencies can be increased by introducing in-plane stresses using plastic deformation [1, 2], thermal gradients [3], or massive wedges [4, 5]. Saw frequencies can also be increased by tapering the saw [6]. The number and locations of slots and holes, which are commonly introduced to relieve the thermal stresses caused by cutting, can be optimized for vibration purposes [7–9].

None of these techniques is applicable to disk drives. High-density magnetic recording requires exceptionally smooth and flat disk surfaces. Tapering the disk or

0022-460X/00/020355 + 21 $35.00/0

introducing slots or holes would degrade the surface geometry and therefore limit recording density. Techniques that introduce in-plane stresses in the disk generally work only if the lowest natural frequency has two or more nodal diameters [10–13]. For circular saws, this is typically the case since saws operate at 60–85% of the first critical speed. However, since disk drives operate at 10–20% of the first critical speed, the lowest natural frequency usually has one nodal diameter, and traditional in-plane stress introduction techniques would actually reduce that frequency [13].

Only the simplest techniques for increasing natural frequencies are applicable to disk drives, and those are often too expensive to employ. For example, disk natural frequencies could be increased by replacing aluminum with a material that is stiffer and lighter, such as glass or ceramics [14]. However, these materials are generally more expensive than aluminum and often have less natural damping. Frequencies could also be raised by strategically constructing the disks from different layers of material [15–17]. Unfortunately, layered disks require additional manufacturing costs and may have bonding imperfections and difficulties. The cost of a 3·5 in aluminum core for a hard disk drive ($\sim$ \$0·30) is almost entirely raw material cost.

Modern disk drives are using thinner and faster rotating disks, both of which reduce the lowest natural frequency. These changes make disk drives more susceptible to vibration-induced recording errors [18]. The long-used design rule that all disk drive vibration resonances be above 500 Hz has become more difficult to achieve, and, in some disk drives, has not been maintained [19]. Yet, despite the pressing need for higher frequency disk designs, most disk drive dynamics research has taken the disk as given and studied the stability of the disk coupled to other disk drive components such as the read/write head [12, 20], the surrounding air [21], or other disks stacked on a spindle [19, 22].

In this paper, we investigate a new disk design that may satisfy the stringent frequency, geometry, and cost requirements of disk drive disks. The design may also be applicable to circular saws or turbines, although that is not the primary focus. In this new design, a pattern of small, dense, internal channels or voids is distributed axisymmetrically about the midplane of the disk. These channels increase the natural frequencies of the disk by removing mass from the midplane of the disk while maintaining the coupling between the deflections of the upper and lower surfaces of the disk. This practice is commonly employed in I-beams and honeycombed sandwich panels, both of whose natural frequencies are higher than those of a corresponding, uniform thickness beam or plate. In fact, manufacturing disk drive disks from a honeycombed sandwich panels was proposed over 25 years ago [23]. A crucial difference between a honeycombed sandwich panel disk and the pattern of channels considered here is that the pattern of channels is potentially moldable from a single casting or stamping operation. Consequently, the cost of a channelled disk may be competitive with that of a uniform disk (or possibly even less expensive, since less material is used). The cost of manufacturing is a crucial issue in determining whether or not the proposed design is practical.

In develping an analytical model for the channelled disk, we assume that the density of channels is sufficiently high such that the disk can be modelled using

variables that are averaged locally over both the channels and the ribs of the disk. This kind of average modelling has been used successfully in the analysis of spiral grooved bearings [24–26]. In this averaged model, the material properties of the channelled disk become orthotropic with the principal axes oriented along the channels [27–29]. This simplification enables us to make quantitative predictions of increased frequencies and optimize the channel design without modelling individual channels and ribs.

Numerical results show that the natural frequencies of a properly channelled disk can be 10–100% higher than those of a uniform disk, depending on the size of the channels. The orientation of the channels does not significantly affect the natural frequencies, but, in the optimal design, the channels do not extend through the whole disk. Instead, they begin at an optimal, central, transition radius and radiate outward to the periphery of the disk.

The paper is organized as follows. In section 2 the averaged model is developed describing the disk geometry, in-plane stresses due to rotation, and bending. Optimal results for both stationary and rotating disks are determined in section 3. In section 4, a simplified model is developed in which only the average thickness and bending rigidity are used. While this model is less detailed than the averaged model, its vibration results are essentially identical to those of the averaged model. In section 5, a finite element analysis is used to determine the magnitude of the surface undulations created by the channels when the disk rotates. These undulations arise from the fact that loads in one direction in a material create strains in the two orthogonal directions for any material in which the Poisson ratio is non-zero. It is determined that for sufficiently dense channels, the surface undulations are at least an order of magnitude below the current flying heights of read/write heads. Finally, in section 6, experimental results are presented which corroborate the numerical predictions.

2. MODELLING

2.1. DISKS GEOMETRY

A thin, circular disk is clamped at inner radius R_i, free at outer radius R_o, and spins about its central axis at a constant angular speed Ω^*. The disk material has density ρ, Young's modulus E, and the Poisson ratio v. Polar co-ordinates (R, θ) are fixed in the stationary frame of reference with the center of the disk at the origin.

In the annulus $R_{ci} \leqslant R \leqslant R_{co}$, a series of evenly spaced rectangular channels symmetrically arranged about the midplane of the disk are carved into the interior of the disk as shown in Figure 1. $\beta(R, \theta)$ is the angle between the channel and a unit vector in the radial direction. The material adjacent to the channel is termed a rib and adjacent channels and ribs are termed channel/rib pairs. The fractional width of a channel/rib pair occupied by the channel is α; the fractional width occupied by the rib is $(1 - \alpha)$. The thickness of each rib is H_r which equals the thickness of the plate in regions of the disk that possess no channels. The height of each channel is H_c. The flexural rigidity of each rib is $D_r = EH_r^3/12(1 - v^2)$.

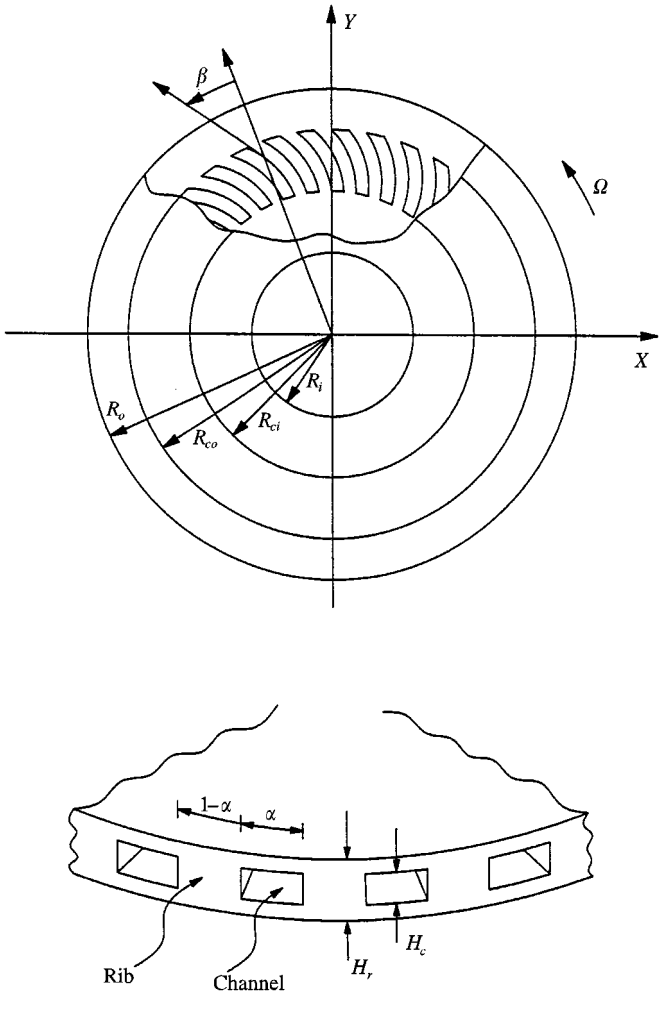

Figure 1. The channelled disk geomtry.

The density of channel/rib pairs is assumed to be sufficiently high such that the behavior of the disk can be modelled using variables that are averaged over each channel/rib pair. Thus, even though the fine structure of the channels rotates, average mass, stiffness and in-plane stresses are determined by the distribution $\beta(R, \theta)$. When $\beta = \beta(R)$ this distribution is axisymmetric, and the average mass, stiffness, and in-plane stresses become independent of the angle of rotation. Although this assumption only approximates the actual system, it provides a framework for the following engineering model.

Define $\bar{N}_r^*$, $\bar{N}_\theta^*$, and $\bar{N}_{r\theta}^*$ as the average in-plane stress resultants across the thickness of the disk and $\bar{W}(R, \theta, T)$ as the average transverse displacement of the disk where T is time. Dimensionless variables are defined by

$$r = R/R_o, \quad t = T\sqrt{D_r/\rho H_r R_o^4}, \qquad \bar{w} = \bar{W}/H_r, \qquad \bar{N} = \bar{N}^* R_o^2/D_r, \tag{1}$$

where the subscripts on $\bar{N}$ and $\bar{N}^*$ have been omitted for brevity. Dimensionless parameters are defined by

$$\kappa = R_i/R_o, \qquad r_{ci} = R_{ci}/R_o, \qquad r_{co} = R_{co}/R_o, \qquad h_c = H_c/H_r, \qquad \Omega = \Omega^* \sqrt{\rho H_r R_0^4/D_r}, \tag{2}$$

and the average dimensionless thickness and flexural rigidity are

$$\bar{h} = \begin{cases} (1-\alpha) + \alpha(1-h_c), & r_{ci} \leqslant r \leqslant {}_{co}, \\ 1, & \kappa \leqslant r \leqslant r_{ci} \text{ and } r_{co} \leqslant r \leqslant 1, \end{cases} \tag{3}$$

$$\bar{D} = \begin{cases} (1-\alpha) + \alpha(1-h_c^3), & r_{ci} \leqslant r \leqslant {}_{co}, \\ 1, & \kappa \leqslant r \leqslant r_{ci} \text{ and } r_{co} \leqslant r \leqslant 1. \end{cases} \tag{4}$$

Calculation of the natural vibration frequencies in two steps. First the in-plane, centripetal stress resultants are determined. Second, these resultants are incorporated into a model describing bending of the disk to determine the natural frequencies.

2.2. STRESSES

The dimensionless plane stress equilibrium equations with a centripetal body force are [30]

$$\bar{N}_{r,r} + \frac{1}{r}\bar{N}_{r\theta,\theta} + \frac{1}{r}(\bar{N}_r - \bar{N}_\theta) = -\bar{h}\Omega^2 r, \tag{5}$$

$$\frac{1}{r}\bar{N}_{\theta,\theta} + \bar{N}_{r\theta,r} + \frac{2}{r}\bar{N}_{r\theta} = 0, \tag{6}$$

where a comma denotes partial differentiation. The average in-plane strains, $\bar{\varepsilon}_r$, $\bar{\varepsilon}_\theta$, and $\bar{\gamma}_{r\theta}$, are related to the average radial and circumferential displacements $\bar{u}$ and $\bar{v}$ by

$$\bar{\varepsilon}_r = \bar{u}_{,r}, \qquad \bar{\varepsilon}_\theta = \bar{u}/r + \bar{v}_{,\theta}/r, \qquad \bar{\gamma}_{r\theta} = \bar{u}_{,\theta}/r + \bar{v}_{,r} - \bar{v}/r. \tag{7}$$

(In order to simplify the following, we normalize the strains and displacements by $12R_o^2/H_r^2$ and $12R_o^3/H_r^2$ respectively.) A constitutive relationship is needed relating the average stress resultants to the average in-plane strains in order to reduce equations (5) and (6) to two differential equations for $\bar{u}$ and $\bar{v}$. Deriving this constitutive relationship is the crux of the modelling.

Consider a small element comprising a single channel/rib pair. Local Cartesian co-ordinates (ξ, η) are aligned with $\hat{\xi}$ tangent to the channel/rib pair. The stresses and strains in the rib in the (ξ, η) co-ordinate system, σ^r_ξ, σ^r_η, $\sigma^r_{\xi\eta}$, ε^r_ξ, ε^r_η, and $\gamma^r_{\xi\eta}$, are assumed to be constant over the rib. The stresses and strains in the channel use the same notation with a superscript c. The stresses and strains in the rib are related by the

dimensionless isotropic plane stress relations

$$\begin{bmatrix} \sigma_\xi^r \\ \sigma_\eta^r \\ \tau_{\xi\eta}^r \end{bmatrix} = \begin{bmatrix} 1 & v & 0 \\ v & 1 & 0 \\ 0 & 0 & (1-v)/2 \end{bmatrix} \begin{bmatrix} \varepsilon_\xi^r \\ \varepsilon_\eta^r \\ \gamma_{\xi\eta}^r \end{bmatrix} \tag{8}$$

and similarly for the channel. We make three assumptions concerning the behavior of the element:

(1) The strains in the $\hat{\xi}$ direction in the rib and the channel are the same, i.e.,

$$\varepsilon_\xi^r = \varepsilon_\xi^c. \tag{9}$$

(2) The total force in the $\hat{\eta}$ direction in the rib and the channel is the same, i.e.,

$$\sigma_\eta^r = \sigma_\eta^c(1 - h_c). \tag{10}$$

(3) The total shear across the channel/rib interface is the same, i.e.,

$$\tau_{\xi\eta}^r = \tau_{\xi\eta}^c(1 - h_c). \tag{11}$$

These assumptions are analogous to treating the rib and channel as springs in parallel in the $\hat{\xi}$ direction and springs in series in the $\hat{\eta}$ direction. Consistent average strains and resultants are then defined by

$$\bar{\varepsilon}_\xi = \varepsilon_\xi^r = \varepsilon_\xi^c, \qquad \bar{\varepsilon}_\eta = (1-\alpha)\varepsilon_\eta^r + \alpha\varepsilon_\eta^c, \qquad \bar{\gamma}_{\xi\eta} = (1-\alpha)\gamma_{\xi\eta}^r + \alpha\gamma_{\xi\eta}^c, \tag{12}$$

$$\bar{N}_\xi = (1-\alpha)\sigma_\xi^r + \alpha(1-h_c)\sigma_\xi^c, \quad \bar{N}_\eta = \sigma_\eta^r = (1-h_c)\sigma_\eta^c, \qquad \bar{N}_{\xi\eta} = \tau_{\xi\eta}^r = (1-h_c)\tau_{\xi\eta}^c. \tag{13}$$

Consider three, separate cases in which a uniform, average strain is applied. When a constant $\bar{\varepsilon}_\xi$ is applied with $\bar{\varepsilon}_\eta = \bar{\gamma}_{\xi\eta} = 0$, the actual strains ε_η^r and ε_η^c must be non-zero in order to satisfy equation (10). These non-zero actual strains are determined from equation (10) and $\bar{\varepsilon}_\eta = 0$. Substituting these values into equations (12) and (13) then gives

$$\bar{N}_\xi = \bar{\varepsilon}_\xi \bar{h}(1 - gv^2), \qquad \bar{N}_\xi = \bar{\varepsilon}_\xi \bar{h}(v - gv^2), \qquad \bar{N}_{\xi\eta} = 0, \tag{14}$$

where

$$g = \frac{\alpha(1-\alpha)h_c^2}{\bar{h}[1-(1-\alpha)h_c]}. \tag{15}$$

When a constant $\bar{\varepsilon}_\eta$ is applied with $\bar{\varepsilon}_\xi = \bar{\gamma}_{\xi\eta} = 0$, equations (12) and (13) give

$$\bar{N}_\xi = \bar{\varepsilon}_\eta \bar{h}(v - gv^2), \qquad \bar{N}_\xi = \bar{\varepsilon}_\eta \bar{h}(1 - g), \qquad \bar{N}_{\xi\eta} = 0. \tag{16}$$

Finally, when a constant $\bar{\gamma}_{\xi\eta}$ is applied with $\bar{\varepsilon}_\xi = \bar{\varepsilon}_\eta = 0$, equations (12) and (13) give

$$\bar{N}_\xi = 0, \qquad \bar{N}_\xi = 0, \qquad \bar{N}_{\xi\eta} = \bar{\gamma}_{\xi\eta}\bar{h}(1-v)(1-g)/2. \tag{17}$$

These three results can be superimposed to give the orthotropic constitutive relation

$$\begin{bmatrix} \bar{N}_\xi \\ \bar{N}_\eta \\ \bar{N}_{\xi\eta} \end{bmatrix} = \bar{h} \begin{bmatrix} (1 - gv^2) & (v - gv^2) & 0 \\ (v - gv^2) & (1 - g) & 0 \\ 0 & 0 & (1 - v)(1 - g)/2 \end{bmatrix} \begin{bmatrix} \bar{\varepsilon}_\xi \\ \bar{\varepsilon}_\eta \\ \bar{\gamma}_{\xi\eta} \end{bmatrix} \tag{18}$$

which reduces to the isotropic case when $g = 0$. Equation (18) can be rotated to give an orthotropic relation in the (r, θ) co-ordinate system [31, 32]:

$$\begin{bmatrix} \bar{N}_\xi \\ \bar{N}_\eta \\ \bar{N}_{\xi\eta} \end{bmatrix} = \bar{h} \begin{bmatrix} (1 + gf_{11}) & (v + gf_{22}) & gf_{13} \\ (v + gf_{12}) & (1 + gf_{22}) & gf_{23} \\ gf_{13} & gf_{23} & (1 - v)/2 + gf_{33} \end{bmatrix} \begin{bmatrix} \bar{\varepsilon}_\xi \\ \bar{\varepsilon}_\eta \\ \bar{\gamma}_{\xi\eta} \end{bmatrix}, \tag{19}$$

where

$$\begin{aligned} f_{11} &= -[5 + 3v^2 - 4(1 - v^2)\cos(2\beta) - (1 - v^2)\cos(4\beta)]/8, \\ f_{12} &= [1 - 8v - v^2 - (1 - v^2)\cos(4\beta)]/8, \\ f_{13} &= (1 - v^2)[2\sin(2\beta) + \sin(4\beta)]/8, \\ f_{22} &= -[5 + 3v^2 + 4(1 - v^2)\cos(2\beta) - (1 - v^2)\cos(4\beta)]/8, \\ f_{23} &= (1 - v^2)[2\sin(2\beta) - \sin(4\beta)]/8, \\ f_{24} &= -(1 - v)[3 - v + (1 + v)\cos(4\beta)]/8. \end{aligned} \tag{20}$$

For the general problem, the boundary conditions are

$$\bar{N}_r = \bar{N}_{r\theta} = 0 \quad \text{at} \quad r = 1, \tag{21}$$

$$\bar{u} = \bar{v} = 0 \quad \text{at} \quad r = \kappa. \tag{22}$$

For our problem, however, we assume that $\beta = \beta(r)$ so the average problem becomes axisymmetric. Consequently, $\bar{u} = \bar{u}(r)$, $\bar{v} = \bar{v}(r)$, $\bar{N}_r \equiv \bar{N}_r(r)$, $\bar{N}_\theta \equiv \bar{N}_\theta(r)$, and $\bar{N}_{r\theta} \equiv 0$. As a result, equation (6) is identically satisfied. By enforcing $\bar{N}_{r\theta} \equiv 0$, one can eliminate $\bar{v}$ and simplify equation (19) to

$$\begin{bmatrix} \bar{N}_\xi \\ \bar{N}_\eta \end{bmatrix} = \bar{h} \begin{bmatrix} 1 + gf_{11} - c_{13}^2/c_{33} & v + gf_{12} - c_{13}c_{23}/c_{33} \\ v + gf_{12} - c_{13}c_{23}/c_{33} & 1 + gf_{22} - c_{23}^2/c_{33} \end{bmatrix} \begin{bmatrix} \bar{u}_{,r} \\ \bar{u}/r \end{bmatrix}, \tag{23}$$

where

$$c_{13} = gf_{13}, \qquad c_{23} = gf_{23}, \qquad c_{33} = (1 - v)/2 + gf_{33}. \tag{24}$$

Equation (23) can then be substituted into equation (5) to give a single differential equation for $\bar{u}$.

2.3. TRANSVERSE DISPLACEMENT

Let the average, dimensionless moments acting on the disk be $\bar{M}_r$, $\bar{M}_\theta$, and $\bar{M}_{r\theta}$. The equation describing the vibration of the disk in the stationary frame of reference,

using classical Kirchhoff plate theory with axisymmetric in-plane stresses [30, 32] is

$$\bar{h}(\bar{w}_{,tt} + 2\Omega\bar{w}_{,t\theta} + \Omega^2\bar{w}_{,\theta\theta}) = (r\bar{N}_r\bar{w}_{,r})_{,r}/r + \bar{N}_\theta\bar{w}_{,\theta\theta}/r^2 + (r^2\bar{M}_{r,r} + 2r\bar{M}_{r\theta,\theta})_{,r}/r^2 - \bar{M}_{\theta,r}/r + \bar{M}_{\theta,\theta\theta}/r^2. \quad (25)$$

Equation (25) can be reduced to a single equation for $\bar{w}$ by formulating a constitutive relation between the average moments and $\bar{w}$. This procedure is analogous to that of section 2.2.

Let the strains in the rib be related to the transverse deflection of the rib w^r according to

$$\varepsilon^r_\xi = -zw^r_{,\xi\xi}, \qquad \varepsilon^r_\eta = -zw^r_{,\eta\eta}, \qquad \gamma^r_{\xi\eta} = -2zw^r_{,\xi\eta}, \quad (26)$$

where z is the co-ordinate perpendicular to the midplane of the disk and $w^r(t, \xi, \eta)$ is independent of z. The resultant moments in the rib are

$$M^r_\xi = \int z\sigma^r_\xi \,\mathrm{d}z, \qquad M^r_\eta = \int z\sigma^r_\eta \,\mathrm{d}z, \qquad M^r_{\xi\eta} = \int z\tau^r_{\xi\eta} \,\mathrm{d}z, \quad (27)$$

where the integral is over the disk thickness. Equations (26) and (27) also apply for the deflections, strains, and moments in the channel with a superscript c. For the channel, equation (26) implies that the disk materials above and below the channel do not move independent of one another. This will only be true for sufficiently dense channels.

We require

$$\varepsilon^r_\xi = \varepsilon^c_\xi, \qquad M^r_\eta = M^c_\eta, \qquad M^r_{\xi\eta} = M^c_{\xi\eta} \quad (28)$$

and define consistent average curvatures and moments by

$$\bar{w}_{,\xi\xi} = w^r_{,\xi\xi} = w^c_{,\xi\xi}, \qquad \bar{w}_{,\eta\eta} = (1-\alpha)w^r_{,\eta\eta} + \alpha w^c_{,\eta\eta},$$
$$\bar{w}_{,\xi\eta} = (1-\alpha)w^r_{,\xi\eta} + \alpha w^c_{,\xi\eta}, \quad (29)$$

$$\bar{M}_\xi = (1-\alpha)M^r_\xi + \alpha M^c_\xi, \qquad \bar{M}_\eta = M^r_\eta = M^c_\eta, \qquad \bar{M}_{\xi\eta} = M^r_{\xi\eta} = M^c_{\xi\eta}. \quad (30)$$

Following an analysis identical to that of section 2.3., we obtain

$$\begin{bmatrix} \bar{M}_r \\ \bar{M}_\theta \\ \bar{M}_{r\theta} \end{bmatrix} = -\bar{D}\begin{bmatrix} 1+df_{11} & v+df_{12} & df_{13} \\ v+df_{12} & 1+df_{22} & df_{23} \\ df_{13} & df_{23} & (1-v)/2+df_{33} \end{bmatrix}\begin{bmatrix} \bar{w}_{,rr} \\ \bar{w}_{,r}/r + \bar{w}_{,\theta\theta}/r^2 \\ 2(\bar{w}_{,\theta}/r)_{,r} \end{bmatrix}, \quad (31)$$

where

$$d = \frac{\alpha(1-\alpha)h_c^6}{\bar{D}[1-(1-\alpha)h_c^3]}. \quad (32)$$

As in the previous section, when a constant $\bar{w}_{,\xi\xi}$ is applied, $w^r_{,\eta\eta}$ and $w^c_{,\eta\eta}$ must be non-zero in order to satisfy the modelling assumptions. These strains make the actual transverse displacement undulate about the mean displacement as one goes across the rib/channel pairs. Substitution of equation (31) into equation (25) gives a single partial differential equation to be solved for $\bar{w}$. Unfortunately, $\bar{M}_{r\theta}$ is in general non-zero so equation (31) cannot be further simplified.

The boundary conditions on $\bar{w}$ are

$$\bar{w} = \bar{w}_{,r} = 0 \quad \text{at } r = \kappa. \tag{33}$$

$$\bar{M}_r = 0 \quad \text{at } r = 1, \tag{34}$$

$$\bar{V}_r \equiv -\bar{M}_{r,r} - \frac{2}{r}\bar{M}_{r\theta,\theta} - \frac{1}{r}(\bar{M}_r - \bar{M}_\theta) = 0 \quad \text{at } r = 1. \tag{35}$$

Dimensionless natural frequencies are obtained using the separable substitution

$$\bar{w}(r, \theta, t) = e^{i(\omega t + n\theta)} w(r), \tag{36}$$

where ω is the natural frequency, n is an integer and $i = \sqrt{-1}$. This leads to the dimensionless eigenvalue problem

$$\begin{aligned}(\omega + n\Omega)^2 \bar{h} w + (r\bar{N}_r w_{,r})_{,r}/r - n^2 \bar{N}_\theta w/r^2 \\ + (r^2 M_{r,r} + 2inr M_{r\theta})_{,r}/r^2 - M_{\theta,r}/r - n^2 M_\theta/r^2 = 0,\end{aligned} \tag{37}$$

where

$$\begin{bmatrix} \bar{M}_r \\ \bar{M}_\theta \\ \bar{M}_{r\theta} \end{bmatrix} = -\bar{D} \begin{bmatrix} 1 + df_{11} & v + df_{12} & df_{13} \\ v + df_{12} & 1 + df_{22} & df_{23} \\ df_{13} & df_{23} & (1 - v)/2 + df_{33} \end{bmatrix} \begin{bmatrix} \bar{w}_{,rr} \\ \bar{w}_{,r}/r - n^2 w/r^2 \\ 2in(w/r)_{,r} \end{bmatrix}. \tag{38}$$

The eigenvalue problem is complex except for $\beta = 0$ or $n = 0$ because $f_{13} \neq 0$ and $f_{23} \neq 0$.

In the sequel, the stresses and natural frequencies are determined using Galerkin's method with eight independent radial polynomials representing $\bar{u}$ and six independent radial polynomials representing w. These representations give frequencies within 1% of those with twice as many degrees of freedom. Although the eigenvalue problem is complex, all computed natural frequencies are real.

3. OPTIMAL CHANNEL DESIGN

3.1. THE STATIONARY DISK

For the stationary disk, the stresses vanish and the natural frequencies are determined by six parameters: κ, r_{ci}, r_{co}, β, α, and h_c. κ is considered a given. Consequently, there are five free parameters available for maximizing the disk's natural frequency.

Calculations support two general conclusions concerning the natural frequencies. First natural frequencies are maximized by $r_{co} = 1$ regardless of the values of the other parameters. Second, changes in β produce negligible changes in the natural frequencies. This second conclusion derives from the fact that the orthotropic behavior of the disk is modulated by the parameter d, which is proportional to h_c^6. For example, when $\alpha = h_c = 0{\cdot}5$, $d = 0{\cdot}0074$. Consequently, changes in the natural frequency are dominated not by the particular pattern of channels cut into the disk, but by the relative ratios of $\bar{D}$ and $\bar{h}$ which determine the relative stiffness and mass of the system.

For $r_{co} = 1$, an optimal value of r_{ci} exists as a function of the other parameters. Figure 2 shows the first five, dimensionless natural frequencies ($n = 0, 1, \ldots, 4$) as a function of r_{ci} for $\kappa = 0{\cdot}3$, $\beta = 0$, and $\alpha = h_c = 0{\cdot}5$. All five frequencies are minimums when $r_{ci} = 1$, which equals the natural frequencies of a disk with no channels. As r_{ci} decreases, the natural frequencies rapidly increase, level off at about a 10% increase, and finally decrease somewhat as r_{ci} approaches κ.

Figure 3 shows the optimal values of r_{ci} as a function of κ for the first five frequencies for $\beta = 0$, and $\alpha = h_c = 0{\cdot}5$. Also shown are the values of r_{ci} at which 60% of the optimal increase is achieved. For $\kappa > 0{\cdot}3$, the optimal value of r_{ci} is essentially the same for all five frequencies and is approximately

$$r_{ci-opt} \sim 0{\cdot}6\kappa + 0{\cdot}4. \tag{39}$$

Since the increase in natural frequency is rapid as r_{ci} initially decreases from one, a substantial fraction of the optimal increase is achieved with relatively short channels. The results show that approximately 2/3 of the total increase in natural frequency is achieved when the channel is approximately 1/3 of its optimal length.

Figure 4(a) shows a contour plot of the percentage increase in the $n = 1$ natural frequency over its value when no channels are present for various values of α and h_c. Figure 4(b) shows a similar contour plot for $n = 3$. The values were computed for $\kappa = 0{\cdot}3$, $r_{ci} = 0{\cdot}57$ (the optimal value), and $\beta = 0$. These two frequencies, $n = 1$ and 3, are representative of all frequencies. In this particular case, the $n = 1$ frequency is the smallest. The increase for $n = 1$ ranges from 0% to approximately 100% depending on the values of α and h_c, while the increase for $n = 3$ ranges from -10 to 60% with in a similar pattern. As expected, higher increases occur for larger values of α and h_c.

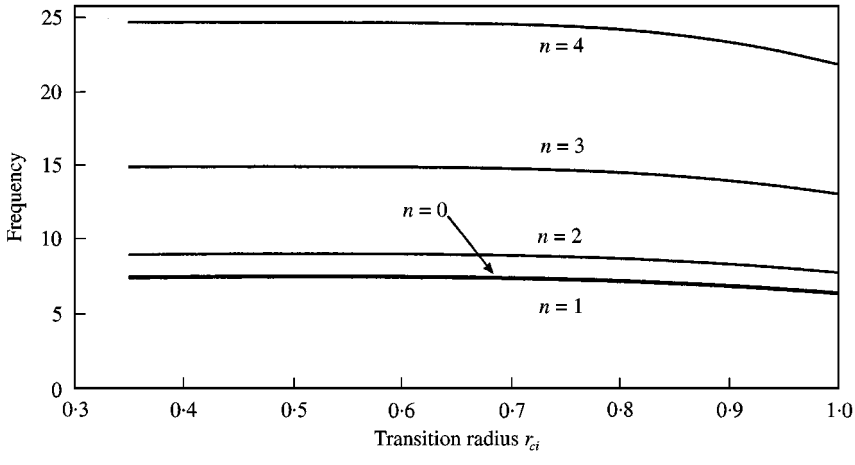

Figure 2. The natural frequencies of the $n = 0$ to 4 vibration modes as a function of the transition radius: $\kappa = 0{\cdot}3$, $\beta = 0$, and $\alpha = h_c = 0{\cdot}5$. $\Omega = 0$.

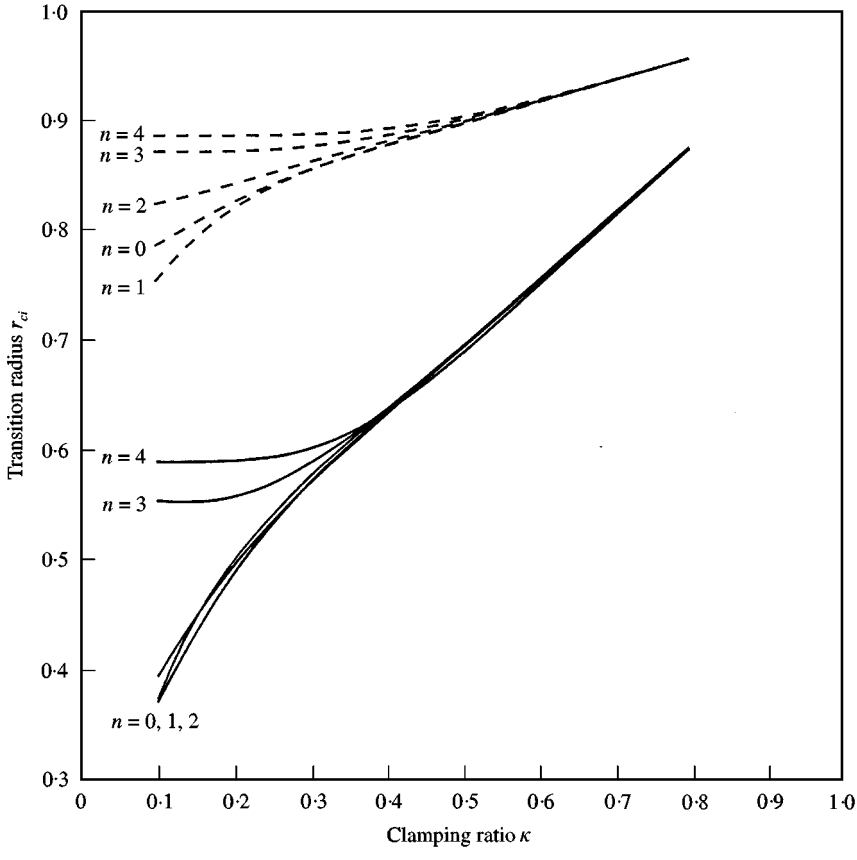

Figure 3. The optimal transition radius (—) for the $n = 0$ to 4 frequencies as a function of κ. The transition radius at which 60% of the maximum increase is achieved is shown by the dashed results.

3.2. THE ROTATING DISK

When the disk rotates, a centripetal stress field is generated in the disk, which is modulated by the presence of the channels. However, the magnitude of this modulation is governed by the parameter g, which is small. Consequently, one anticipates that the principal design parameters for the rotating disk will be r_{ci}, α, and h_c as they were for the stationary disk, that $r_{co} = 1$ will be optimal in all cases and that the effect of β will be negligible.

In fact, this turns out to be the case. For different rotation speeds, the optimal values of r_{ci} are essentially the same as they are for the stationary disk. Figure 5 shows a Campbell diagram displaying the natural frequencies of a channelled ($\alpha = h_c = 0{\cdot}5$, $\beta = 0$, $r_{ci} = 0{\cdot}57$) and unchannelled disk as a function of Ω for $\kappa = 0{\cdot}3$. For clarity, only the modes $n = 0$ to 5 are shown. The presence of the channels increases all frequencies by approximately the same amount regardless of the rotation speed.

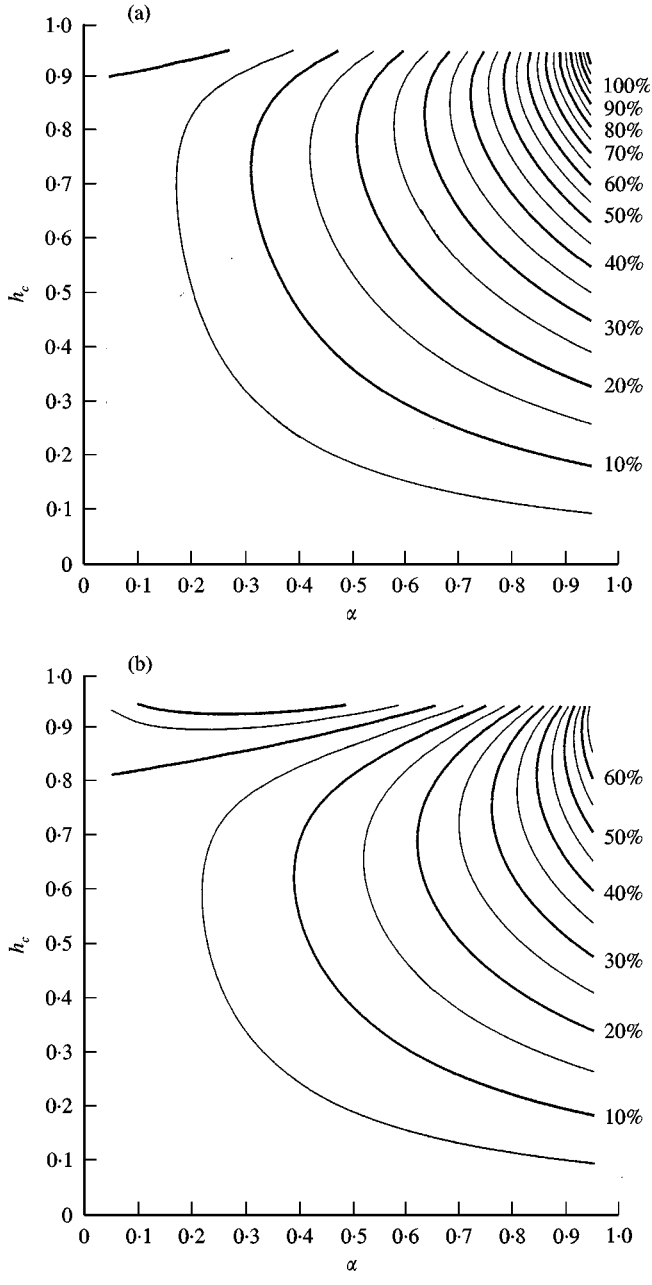

Figure 4. Contour plots of the percentage increase in the (a) $n = 1$ and (b) $n = 3$ frequencies as functions of α and h_c. Contour values are shown on the right.

4. A SIMPLIFIED MODEL

Given the negligible effect of the β on the natural frequencies of the system, it seems likely that acceptable predictions can be made using a simpler model in which only the effects of $\bar{h}$ and $\bar{D}$ are incorporated. This kind of model has been used in the

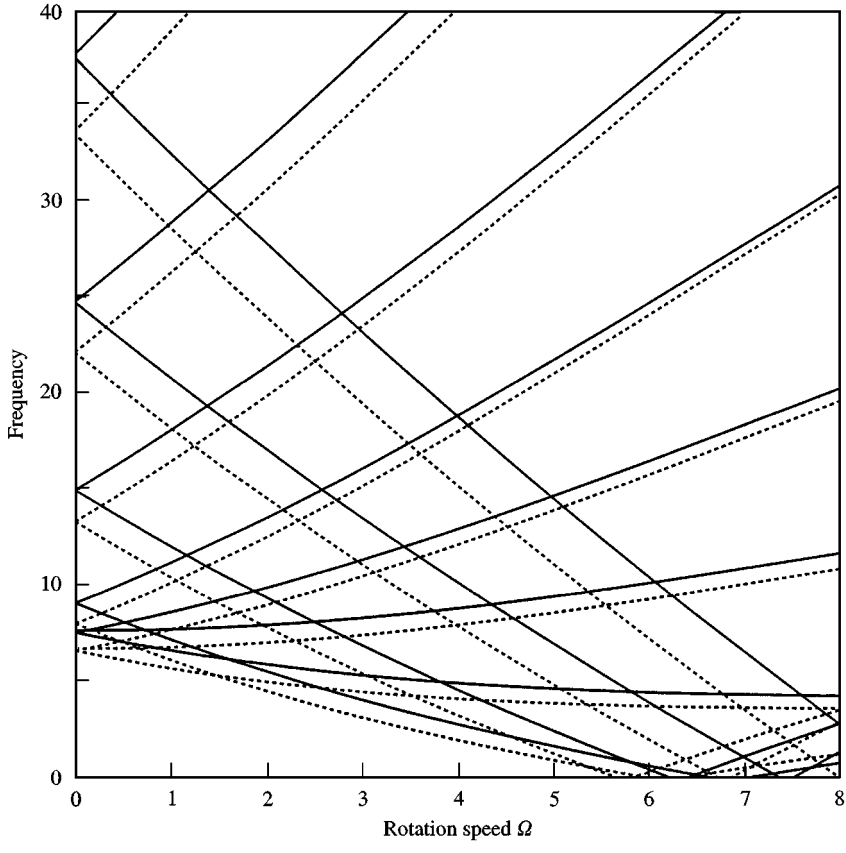

Figure 5. A Campbell diagram showing the natural frequencies of a channelled (—) disk with $\alpha = h_c = 0{\cdot}5$, $\beta = 0$, $r_{ci} = 0{\cdot}57$, and an unchannelled (– – – –) disk as a function of Ω for $\kappa = 0{\cdot}3$. For clarity, only the modes $n = 0$ to 5 are shown.

analysis of disks with stepped, radial profiles. In this model, equation (37) is replaced by

$$(\omega + n\Omega)^2 \bar{h} w + \bar{h}(r\sigma_r w_{,r}/r - n^2 \bar{h}\sigma_\theta w/r^2 - \bar{D}\nabla_n^4 w = 0, \tag{40}$$

where ∇_n^4 is the biharmonic operator for a mode with n nodal diameters. Two different expansions are used for both the stresses and displacements. For $\kappa \leqslant r \leqslant r_{ci}$, the stresses will take the form

$$\sigma_{r(l)} = \Omega^2[a_1/r^2 + b_1 + c_3 r^2], \qquad \sigma_{\theta(l)} = \Omega^2[-a_1/r^2 + b_1 + c_4 r^2], \tag{41}$$

while for $r_{ci} \leqslant r \leqslant 1$, the stresses will be

$$\sigma_{r(2)} = \Omega^2[a_2/r^2 + b_2 + c_3 r^2], \qquad \sigma_{\theta(2)} = \Omega^2[-a_2/r^2 + b_2 + c_4 r^2], \tag{42}$$

where

$$c_3 = -(3 + v)/8, \qquad c_4 = -(1 + 3v)/8. \tag{43}$$

The four constants a_1, b_1, a_2, and b_2 are determined from four stress boundary conditions which prescribe vanishing radial displacement at $r = \kappa$, matching radial

displacement and radial resultant force at $r = r_{ci}$, and vanishing radial stress at $r = 1$. Similarly, the two expansions for w will be determined by the boundary conditions that w and $w_{,r}$ vanish at $r = \kappa$, w, $w_{,r}$, the radial bending moment and shear, are continuous at $r = r_{ci}$, and that the radial bending moment and shear vanish at $r = 1$.

Table 1 compares the natural frequency predictions of the averaged and simplified models for $\Omega = 0$ and 1 for a disk with $\alpha = h_c = 0{\cdot}5$, $\bar{h} = 0{\cdot}75$, $\bar{D} = 0{\cdot}9375$, $\kappa = 0{\cdot}3$, and $r_{ci} = 0{\cdot}57$. In both cases, the differences in the natural frequency predictions for $n = 0$ through $n = 5$ are significantly less than 1%. In other words, despite the additional detail of the averaged model its predictions are essentially identical to those of the simpler model.

The simplified model possesses at least two advantages. First, it is computationally much simpler than the averaged model presented in section 2. Second, it is easy to determine $\bar{h}$ and $\bar{D}$ for non-rectangular channel cross-sections. For example, for channels with circular cross sections,

$$\bar{h} = 1 - \alpha + \alpha(1 - \pi\phi/4), \qquad \bar{D} = 1 - \alpha + \alpha(1 - 3\pi\phi^3/16), \tag{44}$$

where ϕ is the ratio of the channel diameter to H_r and α is the fractional width of the channel along the midplane.

TABLE 1

Frequency comparison of the averaged and simplified model. $\alpha = h_c = 0{\cdot}5$; h-bar $= 0{\cdot}75$; D-bar $= 0{\cdot}9375$: $\kappa = 0{\cdot}3$; $r_{ci} = 0{\cdot}57$

Vibration mode	Uniform disk	Averaged model	Percent increase (%)	Simplified model	Percent increase (%)	Diff. in Inc. (%)
$\Omega = 0$						
(0, 0)	6·66	7·61	14·19	7·61	14·25	− 0·06
(0, 1)	6·55	7·49	14·35	7·50	14·40	− 0·05
(0, 2)	7·96	9·04	13·61	9·05	13·71	− 0·09
(0, 3)	13·28	14·92	12·36	14·94	12·53	− 0·17
(0, 4)	22·07	24·70	11·88	24·74	12·08	− 0·21
(0, 5)	33·56	37·49	11·71	37·56	11·93	− 0·22
$\Omega = 1$						
(0, 0)	6·75	7·69	13·89	7·69	13·93	− 0·04
$(0, 1)_b$	5·67	6·59	16·38	6·60	16·43	− 0·04
$(0, 1)_f$	7·67	8·59	12·11	8·60	12·14	− 0·03
$(0, 2)_b$	6·10	7·16	17·38	7·17	17·53	− 0·15
$(0, 2)_f$	10·10	11·16	10·50	11·17	10·59	− 0·09
$(0, 3)_b$	10·41	12·03	15·54	12·06	15·79	− 0·25
$(0, 3)_f$	16·41	18·03	9·86	18·06	10·02	− 0·16
$(0, 4)_b$	18·20	20·80	14·29	20·85	14·56	− 0·27
$(0, 4)_f$	26·20	28·80	9·92	28·85	10·11	− 0·19
$(0, 5)_b$	28·67	32·58	13·63	32·65	13·90	− 0·27
$(0, 5)_f$	38·67	42·58	10·10	42·65	10·31	− 0·20

Note: Mode (m, n) refers to vibration modes with m nodal circles and n nodal diameters; subscript f refers to forward travelling modes, subscript b to backward travelling modes.

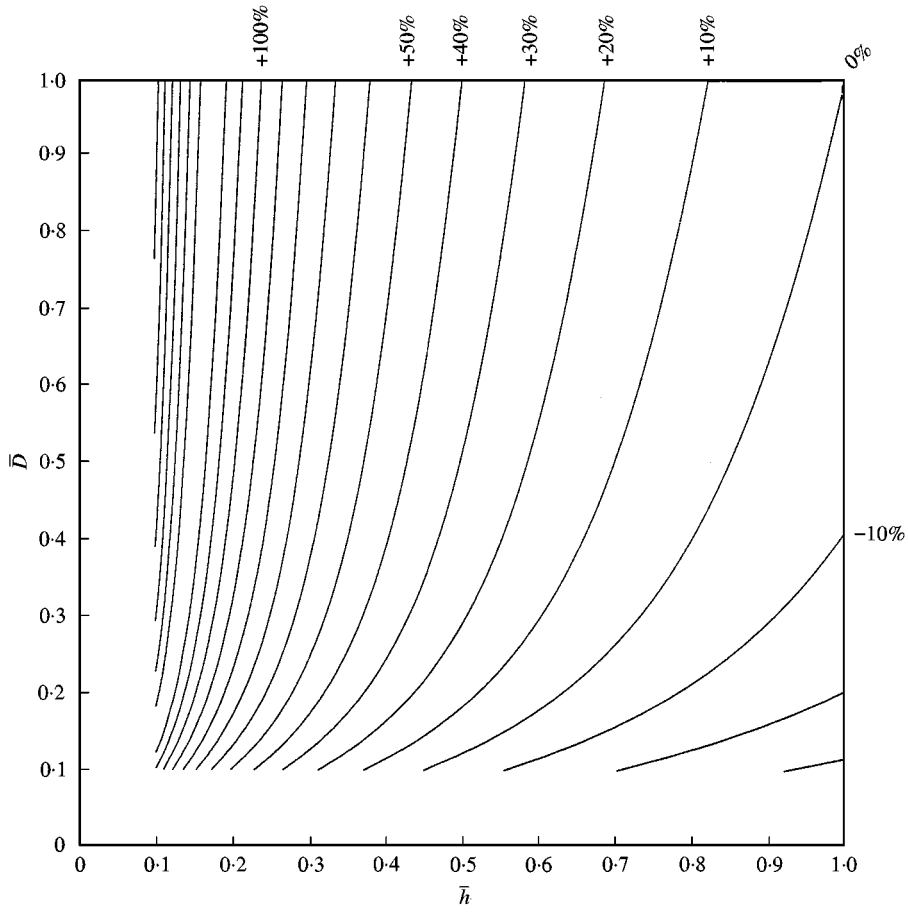

Figure 6. Contour plot of the percentage increase in the $n = 1$ frequency as a function of $\bar{h}$ and $\bar{D}$ using the simplified model: $\kappa = 0{\cdot}3$ and $r_{ci} = 0{\cdot}57$.

Figure 6 shows a contour plot of the percentage increase in the $n = 1$ frequency for $\kappa = 0{\cdot}3$ and $r_{ci} = 0{\cdot}57$ for various values of $\bar{h}$ and $\bar{D}$. This design chart can be used regardless of the channel cross section.

5. SURFACE UNDULATIONS

One potential drawback of internal channels for hard disk drive disks is dimpling of the outer surfaces of the disk. During rotation, the tensile in-plane stresses will cause a contraction of the disk in the transverse direction unless the Poisson ratio is zero. The contraction will be greater over the channels than over the ribs, resulting in an undulating or dimpled surface. Similar undulations will occur in the in-plane distortion of the disk (circular recording tracks of the disk will undulate out of circularity) during bending. Each of these issues needs to be addressed in the design of channeled disks. We present results of the transverse undulations caused by in-plane stresses. The results for in-plane distortions and bending are expected to be qualitatively similar.

In disk drive applications, dimpling and undulations can cause variations in the flying height of the read/write head as the disk spins, which in turn could degrade magnetic recording fidelity. The obvious solution to this is to lap or polish the surface to the necessary flatness while it is rotating. Undulations would then occur when the disk was stationary but not when in use. Another possible solution is to use active control of the recording head actuator to compensate for surface undulations. However, for a disk with 100 channels turning at 6000 r.p.m. the undulation frequency is 10 kHz. Active control of such a high-frequency disturbance is difficult. An alternative solution is to make the channels sufficiently dense that the surface undulations are at least an order of magnitude less than the flying high of the read/write head, which is presently about $2{\cdot}5 \times 10^{-8}$ m (1 microin). The purpose of this section is to calculate the magnitude of the surface undulations in order to prescribe appropriate channel density.

Since surface undulations of a rotating disk are a three-dimensional effect, we abandon the variables of the previous sections, and adopt a new set of dimensionless variables where all lengths have been normalized by R_0 and all stresses by E. Let (r, θ, z) be a polar co-ordinate system with its origin at the center of the disk and the z-axis transverse to the plane of the disk. The dimensionless polar stresses are related to the strains by the three-dimensional, isotropic constitutive relations. The dimensionless centripetal body force acting in the radial direction is

$$F_r = -\omega^2 r, \tag{45}$$

where

$$\omega^2 = \rho(\Omega^*)^2 R_o^2/E. \tag{46}$$

We also define the dimensionless thickness of the disk,

$$h^* = H_r/R_o. \tag{47}$$

The solution of the elasticity problem is proportional to ω^2, so each problem need only be solved for $\omega^2 = 1$ and then scaled appropriately.

Typical values for a 3·5 in aluminum disk drive are $\rho = 2800\ \text{kg/m}^3$, $\Omega^* = 5400$ r.p.m. $R_o = 4{\cdot}8$ cm, $R_i = 1{\cdot}3$ cm, $H_r = 0{\cdot}13$ cm, and $v = 0{\cdot}32$. These give $\omega^2 = 2{\cdot}8 \times 10^{-5}$, $r_i = 0{\cdot}26$, and $h^* = 0{\cdot}017$. Let the dimensionless peak to peak magnitude of the surface undulations in the z direction for $\omega^2 = 1$ be denoted by u_{pp}. Then, if the surface undulations are to be an order of magnitude less than the read/write head flying height, H_f,

$$u_{pp} < (0{\cdot}1)\frac{H_f}{\omega^2 R_o} \sim 2 \times 10^{-3} \tag{48}$$

for the disk described above.

The equations of linear elasticity in cylindrical polar co-ordinates were solved using eight-node, linear, brick finite elements for $r_i = 0{\cdot}26$, and $h^* = 0{\cdot}017$. With $\beta = 0$, one quarter of a rib/channel pair needed to be modelled due to symmetry. Figure 7 shows the mesh used for this problem at a fixed value of r. Vanishing transverse displacements are prescribed along the bottom, $z = 0$ edge, while

vanishing circumferential displacements are prescribed along the left and vertical right edges $\theta = 0$ and $\Delta\theta$. The peak to peak undulation magnitude is the difference in the transverse displacement of the upper left and right corners. In all cases, the channel cross-section is elliptical with $\alpha = 0{\cdot}5$. Two parameters where varied for each run: the fractional height of the channel in comparison with the disk thickness and the angular span, $\Delta\theta$, of the mesh. Since the mesh shown in Figure 7 is a quarter of a channel/rib pair, $\Delta\theta$ represents half the angular span of a channel/rib pair. That is to say, when $\Delta\theta = 1^\circ$, there are 180 channels distributed about the disk.

The mesh shown in Figure 7 was extruded in the r direction to obtain four layers of elements between $r = r_i$ and 1. Consequently, there were 192 elements, 975 degrees of freedom. The results for this mesh were within 15% of values obtained with the element lengths halved (giving eight times as many elements) but took only 2–3 min to solve on an SGI O2 workstation. This accuracy was considered adequate.

Figure 8 shows a contour plot of the peak to peak undulation magnitude, u_{pp}, as functions of the channel height and $\Delta\theta$. As expected, the smallest undulations occur for small channel heights and small $\Delta\theta$. However, for this particular geometry, u_{pp} attains a maximum value for $\Delta\theta$ between 3 and 5°. In order to avoid this maximum, there should always be more than 60 channels in the disk, ideally well more than 60. For example, for $u_{pp} = 0{\cdot}002$ (one-tenth of the flying height) with a channel height of 0·5, $\Delta\theta \sim 1^\circ$, 180 channels in the disk are required. As the channel density increases, u_{pp} decreases rapidly and attains values low enough to for disk drive applications.

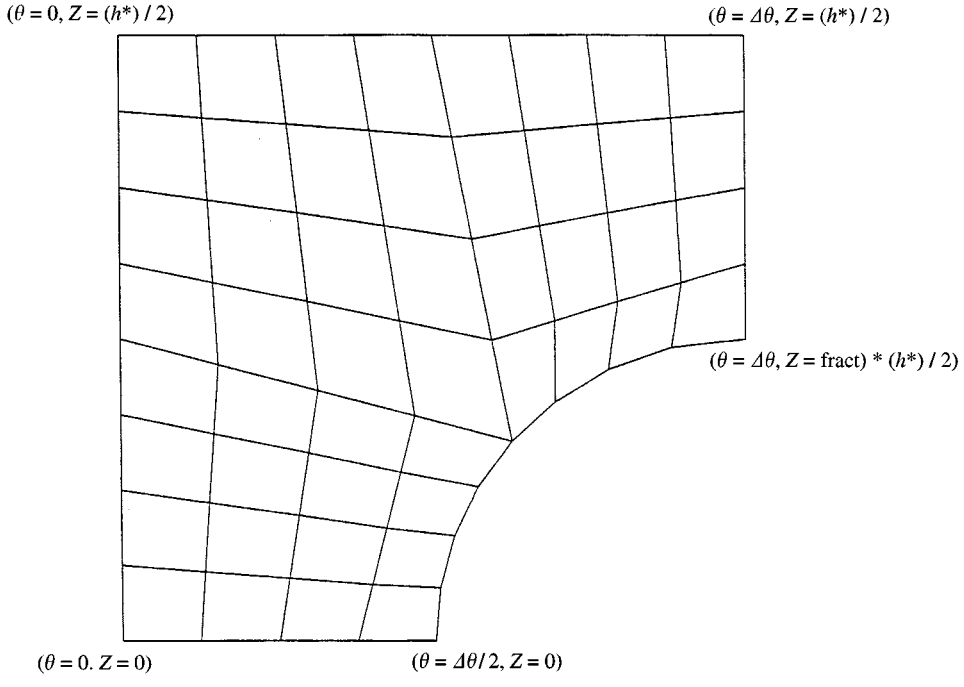

Figure 7. Cross-section of the 3-D finite element model at a fixed radius. The model is a quarter of a channel/rib pair with an elliptical channel cross-section. The co-ordinates of the vertices are given.

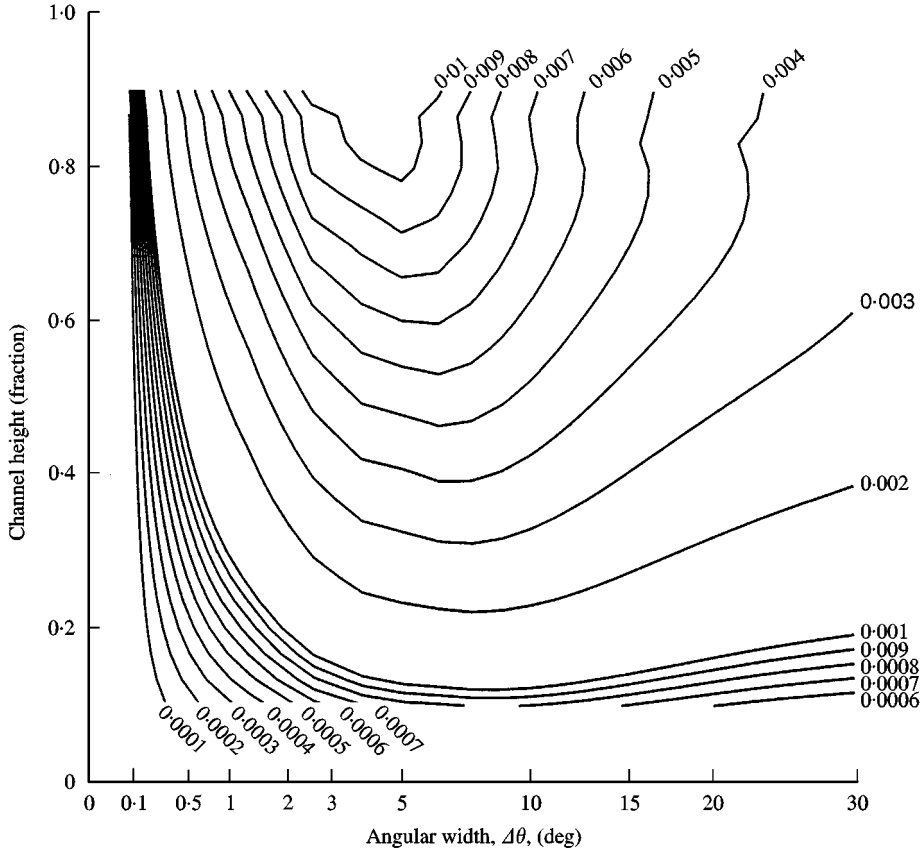

Figure 8. A contour plot of the dimensionless peak to peak surface undulation magnitude for an elliptical channel cross-section as a function of the channel height and the angular width of half a channel/rib pair. The number of channels in the disk is $180/\Delta\theta$.

It should also be mentioned that dimpling could also be reduced by filling the channels with a light, stiff substance that would resist the transverse contraction of the channels. If this substance also had high damping, the damping behavior of the disk could also be significantly increased.

The practicality of the present design depends crucially on two issues: one, the cost of manufacturing the channelled disk, which must be competitive with the extremely inexpensive stamping method used for solid disks; and two, the flatness and lack of distortion of the disk during rotation. The latter issue appears to a challenge that can be overcome with proper design. The former issue, cost, requires further investigation.

6. EXPERIMENTAL CORROBORATION

The numerical predictions were corroborated by measuring the natural frequencies of two different size, thin uniform, aluminum disks when rigidly clamped at $R_i = 38{\cdot}1$ mm (1·5 in). For Disk $\#1$, $H_r = 5{\cdot}08$ mm (0·2 in),

TABLE 2

Experimental results showing the effect of adding radial channels with circular cross-sections to two different disks

Theoretical prediction				Experimental measurements			
Vibration mode	Freq. without channels (Hz)	Freq. with channels (Hz)	Percent increase (%)	Vibration mode	Freq. without channels (Hz)	Freq. with channels (Hz)	Percent increase (%)
Disk #1							
(0, 0)	512	549	7·2	(0, 0)	388	415	7·0
(0, 1)	504	540	7·1	(0, 1)	388	407	4·9
(0, 2)	612	655	7·0	(0, 2)	564	609	8·0
(0, 3)	1021	1092	7·0	(0, 3)	985	1035	5·1
(0, 4)	1698	1817	7·0	(0, 4)	1653	1731	4·7
Disk #2							
(0, 0)	1863	2109	13·2	(0, 0)	1748	1926	10·2
(0, 1)	1895	2145	13·2	(0, 1)	1770	1957	10·6
(0, 2)	2132	2408	12·9	(0, 2)	2176	**	
(0, 3)	2851	3205	12·4	(0, 3)	2504	2692	7·5

Note: Mode (m, n) refers to vibration modes with m nodal circles and n nodal diameters. No (0, 2) mode was found for Disk #2 with channels.

$R_o = 127$ mm (5 in) and $\kappa = 0{\cdot}3$. For Disk #2, $H_r = 5{\cdot}08$ mm (0·2 in), $R_o = 84$ mm (3·3 in), and $\kappa = 0{\cdot}45$.

After measuring the natural frequencies of the uniform disk, channels were formed by drilling 2·54 mm (0·1 in) diameter holes radially ($\beta = 0$) into the outer edge of the disk. For Disk #1, 120 holes were drilled to a depth of 25·4 mm (1 in) giving $r_{ci} = 0{\cdot}8$. For Disk #2, 100 holes were drilled to a depth of 28·9 mm (1·1 in) giving $r_{ci} = 0{\cdot}67$. Because these holes are of constant diameter, the value of α varies with the radial depth of the hole. The average α was 0·43 for Disk #1 and 0·59 for Disk #2. These give $\bar{h} = 0{\cdot}83$ and $\bar{D} = 0{\cdot}97$, and $\bar{h} = 0{\cdot}77$ and $\bar{D} = 0{\cdot}96$ respectively. Although care was taken in drilling these holes, the centerlines of the holes were not precisely on the midplane of the disk. Consequently, the theoretical analysis overestimates $\bar{D}/\bar{h}$ and the increase in natural frequencies.

Analytical predictions and measured results for both disks are shown in Table 2. For Disk #1, the theoretical analysis predicted natural frequency increases of about 7%; experimental increases between 4·7 and 8% were observed. For Disk #2, the theoretical analysis predicted natural frequency increases of about 13%; experimental increase between 7·5 and 10·6% were observed. As expected, the numerical results overestimated the actual increase, but the result qualitatively corroborate the analytical predictions.

7. CONCLUSIONS

(1) Two models are formulated and investigated which predict the natural frequencies of disks with internal channels. First, the influence of the channel is

averaged locally in order to determine the effects of channel orientation and geometry. Second, the average plate thickness and bending rigidity are applied as they would for a stepped disk. The prediction of both models are essentially identical.

(2) In the optimal design, the channels begin at an internal radius and extend outwards to the outer edge of the disk. The orientation of the channels does not matter.

(3) Natural frequency increases of 10–100% are possible depending on the size of the channels. The highest natural frequencies occur when the ratio of $\bar{D}/\bar{h}$ is greatest.

(4) Dimpling of the outer surface can be made less than an order of magnitude of the current read/write head flying height for disk drives provided there are well more than 60 channels in the disk.

(5) Experimental results corroborate the analytical predictions.

(6) Because the optimal design is potentially moldable, channel disk may be competitive with uniform disks for disk drive applications.

REFERENCES

1. C. D. Mote Jr. 1965 *Journal of Engineering for Industry* **87**, 258–264. Free vibration of initially stressed circular disks.
2. G. S. Schajer and C. D. Mote Jr. 1983 *Wood Science and Technology* **17**, 287–302. Analysis of roll tensioning and its influence on circular saw stability.
3. C. D. Mote Jr. and A. Rahimi 1984 *Journal of Dynamic Systems, Measurements and Control* **106**, 123–128. Real time vibration control of rotating circular plates by temperature control and system identification.
4. A. A. Renshaw 1998 *Journal of Sound and Vibration* **210**, 431–439. Increasing the maximum stable rotation speed of a circular disk using speed dependent clamping.
5. H.-R. Kim and A. A. Renshaw 1998 *Journal of Sound and Vibration* **218**, 65–80. Asymmetric, speed dependent tensioning of circular rotating disks.
6. W. M. Bird 1990 *US Patent Number* 4,979,417. Rotating saw blade having improved critical vibrational speed.
7. C. D. Mote Jr. 1972 *Journal of Dynamic Systems, Measurements and Control* **94**, 64–70. Stability control analysis of rotating plates by finite element: emphasis on slots and holes.
8. R. D. Yu and C. D. Mote Jr. 1987 *Journal of Sound and Vibration* **119**, 409–427. Vibration and parametric excitation in asymmetric circular plates under moving loads.
9. R. G. Parker and C. D. Mote Jr. 1991 *Journal of Sound and Vibration* **145**, 95–110. Tuning of the natural frequency spectrum of a circular plate by in-plane stress.
10. H. Lamb and R. V. Southwell 1921 *Proceedings of the Royal Society of London, Series A* **99**, 272–280. The vibrations of a spinning disk.
11. R. V. Southwell 1922 *Proceedings of the Royal Society of London, Series A* **101**, 133–153. On the free transverse vibrations of a uniform circular disc clamped at its centre; and on the effects of rotation.
12. W. D. Iwan and T. L. Moeller 1976 *Journal of Applied Mechanics* **43**, 485–490. The stability of a spinning elastic disk with a transverse load system.
13. A. A. Renshaw and C. D. Mote Jr. 1992 *Journal of Applied Mechanics* **59**, 687–688. Absence of one nodal diameter critical speed modes in an axisymmetric rotating disk.
14. D. J. Perettie, R. T. Fox, A. J. Pyzik, C. Han, P. Macioce and A. Nashif 1996 *Proceedings of the Seventh Annual Information Storage and Processing Systems*

Symposium, *American Society of Mechanical Engineers*, pp. 139–151. Dynamic response and fatigue characterization of aluminum boron carbide ceramic composite materials for disk drive actuator applications.
15. J. P. Knoop, J. R. Weiss and J. C. Uy 1983 *US Patent Number* 4,376,963. Composite magnetic recording disk.
16. A. Frosch, H. Hinkel and G. Kraus 1983 *US Patent Number* 4,415,942. Magnetic disk substrate of fiber-reinforced plastic.
17. T. Bayer, H. Hinkel, K. Kleischmann, U. Kuenzel and Schafer 1986. *US Patent Number* 4,598,017. Composite magnetic disk with SI and SIC substrate.
18. J. S. McAllister 1996 *Sound and Vibration* **30** 24–28. The effect of platter resonances on track misregistration in disk drives.
19. I. Y. Shen and C.-P. R. Ku 1997 *Journal of Applied Mechanics* **64**, 165–174. A nonclassical vibration analysis of a multiple rotating disk and spindle assembly.
20. W. D. Iwan and K. J. Stahl 1973 *Journal of Applied Mechanics* **95**, 445–451. The response of an elastic disk with a moving mass system.
21. A. A. Renshaw 1998 *Journal of Applied Mechanics* **65**, 116–120. Critical speed for floopy disks.
22. J. G. Tseng and J. A. Wickert 1998 *Journal of Vibration and Acoustics* **120**, 234–239. Split vibration modes in acoustically-coupled disk stacks.
23. R. A. Rosenblum 1972 *US Patent Number* 3,646,533. Rotary disk assembly having low-density core for information storage.
24. S. B. Malanoski and C. H. T. Pan 1965 *Journal of Basic Engineering* **87**, 547–558. The static and dynamic characteristics of the spiral-grooved thrust bearing.
25. J. H. Vohr and C. Y. Chow 1969 *Journal of Lubrication Technology* **91**, 675–686. Helical-grooved journal bearing operated in turbulent regime.
26. Y. Zang and M. R. Hatch 1996 *Proceedings of the Seventh Annual Information Storage and Processing Systems Symposium*, *American Society of Mechanical Engineers*, 73–84. On the whirl dynamics of hydrodynamics bearing spindle in information storage systems.
27. H. C. Loh and J. F. Carney III 1977 *Journal of Applied Mechanics* **99**, 499–501. Vibration and stability of spinning annular plates reinforced with edge beams.
28. C. T. Dyka and J. F. Carney III 1979 *Journal of Sound and Vibration* **64**, 223–231. Vibration and stability of spinning polar orthotropic annular plates reinforced with edge beams.
29. L.-W. Chen and J.-R. Hwang 1988 *Journal of Sound and Vibration* **125**, 555–563. Axisymmetric dynamic stability of polar orthotropic thick circular plates.
30. J. L. Nowinski 1964 *Journal of Applied Mechanics* **31**, 72–78. Nonlinear transverse vibrations of a spinning disk.
31. R. M. Jones 1975 *Mechanics of Composite Materials*. Washington, D.C: Scripta Book Company.
32. E. H. Mansfield 1989 *The Bending and Stretching of Plates*. Cambridge: Cambridge University Press.